Vessel Segmentation with Automatic Centerline Extraction Using Tubular Tree Segmentation

Vandana Mohan[1], Ganesh Sundaramoorthi[1,2], Arthur Stillman[3], and Allen Tannenbaum[1]

[1] School of Electrical and Computer Engineering, Georgia Institute of Techology, Atlanta, GA, USA gth115a@mail.gatech.edu,
[2] Computer Science Department, University of California, Los Angeles, CA, USA,
[3] Department of Radiology, Emory University, Atlanta, GA, USA.

Abstract. The study of the coronary vessel structure is crucial to the diagnosis of atherosclerosis and other cardiovascular diseases, which together account for $\sim 35\%$ of all deaths in the United States per year. Vessel Segmentation from CTA data is challenging because of non-uniform image intensity along the vessel, and the branching and thinning geometry of the vessel tree. We present a novel method for vessel extraction that models the vasculature as a tubular tree and individual vessels as 3D tubes. We create an initial tube from a few seed points within the vessel tree, and then evolve this initial tube using a variational energy optimization approach to capture the vessel while automatically detecting branches in the vessel tree. A significant advantage of our proposed framework is that the center-line of the blood vessel tree, which is useful in defining cross sectional area of the vessel and evaluating stenoses, is detected automatically as the tubular tree evolves. Existing approaches on the other hand need an explicit step for skeletonization of the vessel volume after segmentation. Another benefit is that the parent-child relationships between branches are also automatically obtained, which is useful in fly-through visualization as well as clinical reporting.

1 Introduction

Blood vessel segmentation is vital to surgery planning and the diagnosis of cardiovascular disorders such as atherosclerosis. Segmentation using only intensity information from CTA data is insufficient since variations in contrast along the vessel and local ambiguities in intensity can cause leakages to occur. However using shape priors for vessel segmentation is challenging because diseased vessels can have different and abnormal shapes. In this work, we propose a model for a tubular surface as a center-line coupled with a radius function. We build energy functionals using this representation which we optimize using a variational approach. Casting vessel segmentation in this framework introduces a "soft" tubular shape prior. The center-line obtained is the skeleton of the vessel tree, which facilitates fly-through visualization to gauge plaque deposits and stenosis in the vessel interior. We also gain computational efficiency since the problem of segmenting a closed surface in 3D is transformed into the segmentation of a 4D open curve and the use of a parametric curve evolution approach for this 4D curve is more efficient than levelset-based approaches such as in [1].

2 Related work

We give a brief review of several relevant geometric techniques based on deformable models pioneered by [2]) for vessel extraction. In [3], the authors approximate the evolution of a one-dimensional curve embedded in 3D space based on edge information of the image to segment vessels. In [4], a flux-maximizing flow on curves/surfaces is constructed to align the curve/surface normal along the gradient direction of the image and is implemented with level set methods. To take into account the geometrical shape of a vessel, the authors of [5] construct a geometric shape prior to favor vessel-like structures and combine it with image region statistics to deform the curve/surface to capture the vessel. In [6], a level set method is used based on histogram information to deform an initialized vessel tree that was obtained by registration of the image to a pre-segmented reference image. These methods do not explicitly model the tubular nature of the vessel(s) to be detected. Therefore in [7], the authors model vessel surfaces as the envelope of a collection of spheres, thus having a explicit tube-like model for the vessel. The segmentation is performed based on a minimal path technique [8]. The centerline is thus detected without any additional effort in comparison to methods which process the segmentation to obtain a centerline (e.g. [9]). The method of [7] requires that the user inputs the endpoints of the vessel branch.

In this present work, we model an individual vessel as a tube-like surface that evolves to detect the vessel. We do not require that the endpoints of the vessel are known or fixed during the evolution. Also, while branch detection has previously been dealt with as a problem of detecting branch points given a skeleton or the segmented surface (e.g. [10],[11],[12]), our method automatically detects branches and generates new tube-like surfaces to segment vessel branches, yielding a tubular tree structure for the overall segmentation. We present the details of the framework in Section 3 and discuss the experiments and results in Section 4.

3 Tubular Tree Segmentation framework

3.1 Tubular Surface model

We represent the vasculature as a tubular tree and model each individual vessel as a tubular surface determined by a center line and a radius function defined at each point of this center-line, akin to the model of Mohan et al [13]. Given an open curve $c : [0,1] \to \mathbb{R}^3$, the center line, and a function $r : [0,1] \to \mathbb{R}^+$, the radius function, we can define the tubular surface, $S : \mathbb{S}^1 \times [0,1] \to \mathbb{R}^3$ ($\mathbb{S}^1$ is $[0, 2\pi]$ with endpoints identified) as:

$$S(\theta, u) = c(u) + r(u)[n_1(u)\cos\theta + n_2(u)\sin\theta] \tag{1}$$

where $n_1, n_2 : [0,1] \to \mathbb{R}^3$ are normals to the curve c defined to be orthonormal, smooth, and such that the dot products $c'(u) \cdot n_i(u)$ vanish. See Figure 1 for an illustration of a tubular surface. The tubular surface is represented as a collection of circles each lying in the plane perpendicular to the center line $\tilde{c} : [0,1] \to \mathbb{R}^4$:

$$\tilde{c}(u) = (c(u), r(u))^T. \tag{2}$$

Note that we significantly extend the work of Mohan et al [13] since it is the stable evolution of end points (Section 3.4) and the novel automatic branch detection algorithm (Section 3.5) put forth in this work that allow the model to be applied to the

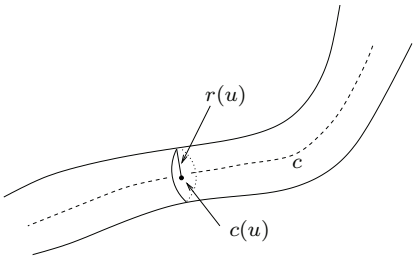

Fig. 1: Illustration of Tubular Surface model

segmentation of Tubular Trees and practically usable for vessel segmentation. We also propose a new energy suitable for vessel segmentation (Section 3.2) which is tailored to CT imagery versus the MRI imagery used in [13].

3.2 Energy for Vessel Segmentation

We define an energy functional on tubes such that the optimum tube corresponds to the vessel of interest. Since tubes are identified with 4D space curves in our method, we define energies directly on 4D curves. Let $\Psi : \mathbb{R}^4 \times S^2 \to \mathbb{R}^+$ ($\Psi(x, r, v) \in \mathbb{R}^+$) be a weighting function to be chosen, and we define the energy as

$$E(\tilde{c}) = \int_{\tilde{c}} \Psi(\tilde{c}(\tilde{s}), \frac{c'(\tilde{s})}{|c'(\tilde{s})|}) \, \mathrm{d}\tilde{s}, \;\; \tilde{c} = (c, r) \tag{3}$$

where $\mathrm{d}\tilde{s} = |\tilde{c}'(u)| \, \mathrm{d}u = \sqrt{(r'(u))^2 + |c'(u)|^2} \, \mathrm{d}u$ is the arclength measure of the 4D curve, and $c'(\tilde{s})/|c'(\tilde{s})|$ is the unit tangent to c, the center line. The term $\mathrm{d}\tilde{s}$ penalizes the non-smoothness of the center line and the radius function. The energy (3) is related to the length of a curve in a Finsler manifold [14–16].

The weighting function, Ψ, is chosen to maximize the difference in mean intensities inside and outside the discs centered along the center-line. This is given as following:

$$\Psi(\tilde{p}, v) = \mu_{D(\tilde{p},v)} - \mu_{D((p,\alpha r),v)\setminus D(\tilde{p},v)} \tag{4}$$

where $\tilde{p}$ is the 4D position along the curve, v is the tangential directions along the curve and μ's are means:

$$\mu_{D(\tilde{p},v)}(\hat{v}) = \frac{1}{r^2} \int_{D(\tilde{p},v)} I(x) \, \mathrm{d}A(x) \tag{5}$$

$$\mu_{D((p,\alpha r),v)\setminus D(\tilde{p},v)}(\hat{v}) = \frac{1}{(\alpha^2 - 1)r^2} \int_{D((p,\alpha r),v)\setminus D(\tilde{p},v)} I(x) \, \mathrm{d}A(x), \tag{6}$$

where $\mathrm{d}A$ is the area element and $I(x) \in \mathbb{R}^+$ is the image intensity at a given position x. Notice that the energy (to be maximized) uses *local* region-based statistics to separate the tube's interior and exterior in comparison to traditional region-based approaches which separate the global mean intensities inside and outside the surface (e.g. [17]). It is thus suited to vessel structures where the image intensity varies smoothly along a vessel (but is not necessarily constant). Note also the dependence of Ψ on $\hat{v}$, which is the orientation of the disk.

3.3 Optimization by variational approach

The energy functional (3) is optimized using a steepest ascent flow. By maximizing (3), we are maximizing a weighted length and this process is unstable using traditional gradient ascent because such a gradient flow results in a reverse heat diffusion. As discussed in the work of Mohan et al [13], such energies may be optimized by using a gradient ascent flow derived from a Sobolev-type metric [18] (different from the traditional gradient flow technique that is based on an $\mathbb{L}^2$-type metric), which results in a stable ascent flow. The gradient ascent of (3) which we use to evolve the tubes is

$$\frac{1}{L}\nabla_{\text{Sob}}E(\tilde{c}) = K(\Psi_{\tilde{p}}) + \partial_{\hat{s}}K(\hat{\Psi}_v\sqrt{1+(r_{\tilde{s}}/|c_{\tilde{s}}|)^2} + \Psi\tilde{c}_{\tilde{s}}), \tag{7}$$

where

$$K(f) := \int_0^L K(\cdot,\tilde{s})f(\tilde{s})\,\mathrm{d}\tilde{s}, \quad K(\tilde{s}_1,\tilde{s}_2) = \frac{1}{L}\begin{cases}\frac{\tilde{s}_2}{L}(1-\frac{\tilde{s}_1}{L}) & 0\le\tilde{s}_2\le\tilde{s}_1\\ \frac{\tilde{s}_1}{L}(1-\frac{\tilde{s}_2}{L}) & \tilde{s}_1\le\tilde{s}_2\le L\end{cases}. \tag{8}$$

Note that as stated in [18], (7) can be computed efficiently in order N complexity, N being the number of sample points of the curve.

3.4 Moving end points

For vessel segmentation, we wish to initialize a few seed points in frames where the vessel cross sections are visible and then grow this initial tube to capture the entire vessel structure including branches. While in the work of Mohan et al [13], the gradient ascent of (3) was proposed for extracting the cingulum bundle in DW-MRI using an initial guess of its centerline such that the endpoints of the 4D curve were fixed, we must be able to evolve the end points (end disks of the tube). To do this, we compute the variation of the energy with respect to the endpoints of the 4D curve. Thus in our work, the endpoints are evolved according to

$$\tilde{c}_t(0) = \mp\hat{\Psi}_v\sqrt{1+\left(\frac{r_{\tilde{s}}}{|c_{\tilde{s}}|}\right)^2} \mp \Psi\tilde{c}_{\tilde{s}},\ \tilde{c}_t(1) = \pm\hat{\Psi}_v\sqrt{1+\left(\frac{r_{\tilde{s}}}{|c_{\tilde{s}}|}\right)^2} \pm \Psi\tilde{c}_{\tilde{s}}. \tag{9}$$

To maximize the energy of a single tube, we alternatively evolve the endpoints of the 4D curve using (9) and its interior using (7). Note that we achieve stability in evolving the end points outward (i.e increasing length) by the use of the Sobolev norm-based gradient flow [18].

3.5 Automatic branching detection in vessel tree

The branching geometry of the blood vessel tree poses a challenge in applying the tubular surface extraction framework to vessel segmentation. We wish to detect the presence of branches in the vicinity of the evolving structure, as it grows out, and then construct new tube(s) to capture the detected vessel branches. We propose a novel branch detection algorithm (Algorithm 1) which is performed for each end point in the tree each time it moves significantly.

Algorithm 1 Branch detection algorithm

Construct a sphere S^2 of radius R (a function of the input guess for typical vessel radius) centered at the end point under analysis.
Sample N directions $d_i(i = 1toN)$ uniformly off this sphere S^2.
Construct tubes of radius 1 and length R along each of the N directions, originating at the end point under analysis.
Estimate the mean image intensity within each tube as $I_{mean}(d_i)$.
Threshold the estimated mean intensities with respect to the parent branch intensity I_{thres}.
Extract the subset of directions d_i off the sphere S^2 with mean intensities above the threshold.
Apply k-means clustering [19,20] to the extracted directions $d_i \forall i \in (1, N) and I_{mean}(d_i) >= I_{thres}$, with a target of 3 clusters.
if Number of non-empty clusters < 3 **then**
  Declare non-existence of branching at end point under analysis
else
  Compute the centroid of the directions in each cluster, to yield 3 candidate branch directions.
  Eliminate the direction that has maximum overlap with the parent branch's volume.
  Compute the dot products of the 2 remaining candidate directions with the tangent of the parent branch at the end point.
  Extend the parent branch by the candidate direction better aligned with the tangent at the end point.
  Create a new branch in the tree structure using the 1 remaining candidate direction.
end if

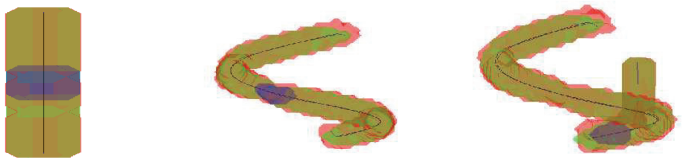

Fig. 2: Results of experiments on synthetic curvilinear structures: the target structure (green), segmentation result (red), extracted center-line (black), true centerline (blue), and initial volume (blue).

4 Experiments and Results

4.1 Synthetic images

The proposed framework was applied to synthetic images with curvilinear and branched structures. The set-symmetric difference of the result with respect to ground truth was found to be $\sim 4\%$ across different synthetic structures of average radius 3 voxels. Figure 2 shows the ground truth, segmentation results and associated center-line for selected experiments.

4.2 CTA Cardiac Images

The algorithm was tested on a population of cardiac data sets acquired from a Siemens Sensation 64 slice CTA machine. The framework is initialized with 1 user-input point at the root of the vessel tree, and a *guess* for typical vessel radius which guides the branch detection process.

Fig. 3: 3D Visualization of the extracted vessel tree for Case 1 with segmentation result (red), extracted center-line (green) and initialization (blue)

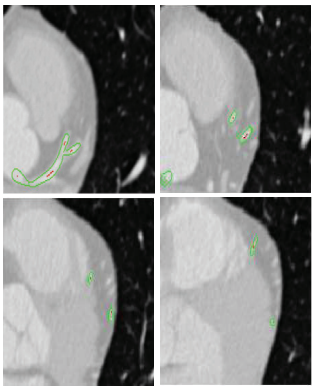

Fig. 4: Slicewise views of the vessel segmentation result for Case 1

We show here the results for three of the many data sets tested on, for the Left Anterior Descending (LAD) coronary artery. Figures 3 and 5 show the 3D visualization of the segmented vessel trees for two cases. Also shown in these figures is the extracted center-line. *Note that no additional processing was required to obtain this center-line*. The algorithm captures the branching structure automatically and successfully handles the thinning structure of the vessel tree, from the root to tips. Figures 4 and 6 show the corresponding slice-wise views of the segmentation result. We can clearly see that the framework copes well with the non-uniform contrast within the vessel volume, and is capable of following an entire vessel ~ 200 voxels in length, from the simple 1-point input (with stability as a natural outcome of using the Sobolev norm). Finally in Figure 7, we show the tubular tree evolving in 3D for a third case, illustrating how the branch detection works to capture the entire tree. The results have been qualitatively validated by medical collaborators.

An important potential application of our framework is that since the 3D skeleton and the associated radius function are direct outputs of the model, we can do a preliminary stenosis evaluation by looking for local minima of the radius function along the center-line. We show a proof-of-concept of this idea in Figure 8 which shows the cross-sectional area of one of the branches of the extracted vessel tree shown in Figure 3 and reveals a site of mild stenosis (40% blockage) (corresponding to the minimum of the plotted curve).

5 Conclusion

In this work, we present a novel framework for extracting tubular, branched anatomical structures that *simultaneously returns the segmented volume and the 3D skeleton for the structure (with the parent-child relationships of the branches in the vessel tree)* starting from a simple 1-point initialization. We have shown that the framework is successful in segmenting blood vessels from cardiac CTA imagery of multiple subjects. The use of statistics over *local* regions implies that the segmentation result is a smooth surface. The framework also returns the parent-child relationships in the vasculature's tree structure

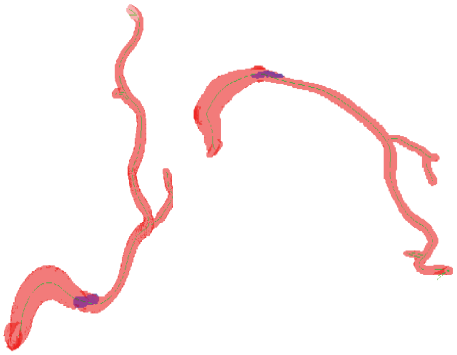

Fig. 5: 3D Visualization of the extracted vessel tree for Case 2 with segmentation result (red), extracted centerline (green) and initialization (blue)

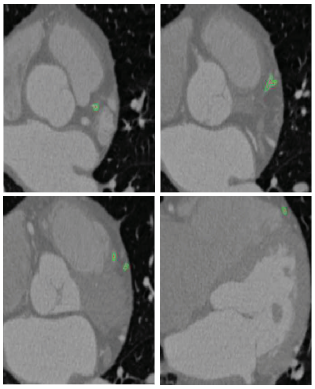

Fig. 6: Slicewise views of the vessel segmentation result for Case 2

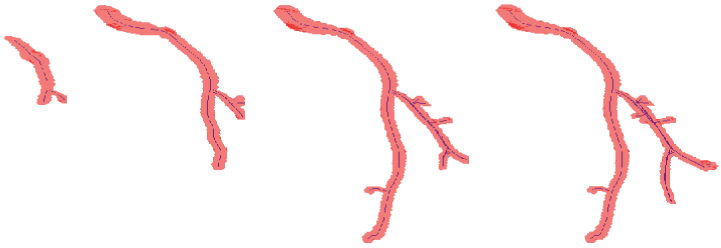

Fig. 7: Visualization of the evolving tubular tree in 3D for Case 3: evolving volume (red), centerline (blue)

automatically, which is extremely useful in clinical reporting and in further analysis such as plaque detection. In future work, we plan to leverage these advantages and apply the proposed framework in soft plaque detection, as well as explore in-depth its potential in stenosis evaluation.

References

1. Nain, D., Yezzi, A., Turk, G.: Vessel Segmentation Using a Shape Driven Flow. LECTURE NOTES IN COMPUTER SCIENCE (2004) 51–59
2. Kass, M., Witkin, A.P., Terzopoulos, D.: Snakes: Active contour models. International Journal of Computer Vision **1**(4) (1988) 321–331
3. Lorigo, L.M., Grimson, W.E.L., Faugeras, O.D., Keriven, R., Kikinis, R., Nabavi, A., Westin, C.F.: Codimension - two geodesic active contours for the segmentation of tubular structures. In: CVPR, IEEE Computer Society (2000) 1444–1451

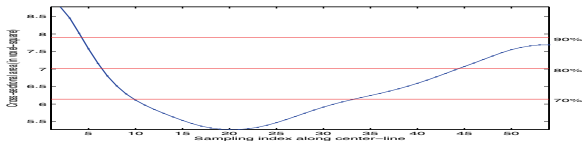

Fig. 8: Cross-sectional area along vessel shown in Figure 3. The left y-axis shows cross-sectional area in voxel-square and the red lines highlight the values of area that correspond to stenosis percentages shown on the right y-axis. (Note that the minimum of this curve indicates a site of mild stenosis.)

4. Vasilevskiy, A., Siddiqi, K.: Flux maximizing geometric flows. IEEE Trans. Pattern Anal. Mach. Intell. **24**(12) (2002) 1565–1578
5. Nain, D., Yezzi, A.J., Turk, G.: Vessel segmentation using a shape driven flow. In Barillot, C., Haynor, D.R., Hellier, P., eds.: MICCAI (1). Volume 3216 of Lecture Notes in Computer Science., Springer (2004) 51–59
6. Manniesing, R., Velthuis, B., van Leeuwen, M., van der Schaaf, I., van Laar, P., Niessen, W.: Level set based cerebral vasculature segmentation and diameter quantification in ct angiography. Medical Image Analysis (2006)
7. Li, H., Yezzi, A.: Vessels as 4-d curves: Global minimal 4-d paths to extract 3-d tubular surfaces and centerlines. IEEE Transactions on Medical Imaging **26**(9) (2007) 1213–1223
8. Cohen, L.D., Kimmel, R.: Global minimum for active contour models: A minimal path approach. In: CVPR, IEEE Computer Society (1996) 666–673
9. Bouix, S., Siddiqi, K., Tannenbaum, A.: Flux driven automatic centerline extraction. Medical Image Analysis **9**(3) (2005) 209–221
10. Zhu, L., Haker, S., Tannenbaum, A.: Flattening Maps for the Visualization of Multibranched Vessels. IEEE Transactions on Medical Imaging **24**(2) (2005) 191–198
11. Wang, L., Bhalerao, A.: Model Based Detection of Branching Structures. Proc. Medical Image Understanding and Analysis, Portsmouth, UK (2002)
12. Yang, Y., Zhu, L., Haker, S., Tannenbaum, A., Giddens, D.: Harmonic skeleton guided evaluation of stenoses in human coronary arteries. Lecture Notes in Computer Science **3749** (2005) 490
13. Mohan, V., Sundaramoorthi, G., Melonakos, J., Niethammer, M., Kubicki, M., Tannenbaum, A.: Tubular Surface Evolution for Segmentation of the Cingulum Bundle From DW-MRI. MFCA08 150
14. Pichon, E.: Novel methods for multidimensional image segmentation. (2005)
15. Pichon, E., Westin, C.F., Tannenbaum, A.: Anisotropic conformal flows and dt-mri tractography. In: MICCAI. (2005)
16. Melonakos, J., Pichon, E., Angenent, S., Tannenbaum, A.: Finsler active contours. IEEE Transactions on Pattern Analysis and Machine Intelligence (To Appear)
17. Chan, T., Vese, L.: Active contours without edges. Image Processing, IEEE Transactions on **10**(2) (2001) 266–277
18. Sundaramoorthi, G., Yezzi, A.J., Mennucci, A., Sapiro, G.: New possibilities with Sobolev active contours. In: SSVM. (2007) 153–164
19. Kanungo, T., Mount, D., Netanyahu, N., Piatko, C., Silverman, R., Wu, A.: An Efficient k-Means Clustering Algorithm: Analysis and Implementation. IEEE Transactions on Pattern Analysis and Machine Intelligence (2002) 881–892
20. Hartigan, J., Wong, M.: A K-means clustering algorithm. JR Stat. Soc. Ser. C-Appl. Stat **28** (1979) 100–108